CrossMark

ORIGINAL PAPER

LiNi$_{0.5}$Mn$_{1.5}$O$_4$ hollow nano-micro hierarchical microspheres as advanced cathode for lithium ion batteries

Yao Xiao[1] · Yanfang Zhu[1] · Tuo Gao[2] · Benhe Zhong[1] · Xiaodong Guo[1,3]

Abstract The high-voltage spinel-type LiNi$_{0.5}$Mn$_{1.5}$O$_4$ (LNMO) is a promising cathode material for next-generation lithium ion batteries. In this study, hollow LNMO microspheres have been synthesized via co-precipitation method accompanied with high-temperature calcinations. The physical and electrochemical properties of the materials are characterized by x-ray diffraction (XRD), TGA, RAMAN, CV, scanning electron microscope (SEM), transmission electon microscopy (TEM), electrochemical impendence spectroscopy (EIS), and charge-discharge tests. The results prove that the microspheres combine hollow structures inward and own a cubic spinel structure with space group of *Fd*-3*m*, high crystallinity, and excellent electrochemical performances. With the short Li$^+$ diffusion length and hollow structure, the hierarchical LNMO microspheres exhibit 138.2 and 108.5 mAh g^{-1} at 0.5 and 10 C, respectively. Excellent cycle stability is also demonstrated with more than 98.8 and 88.2 % capacity retention after 100 cycles at 1 and 10 C, respectively.

Keywords Spinel lithium nickel manganese oxides · Hollow structure · Cathode materials · Lithium ion batteries

✉ Xiaodong Guo
  xiaodong2009@163.com

[1] College of Chemical Engineering, Sichuan University, No. 24 South Section 1, Yihuan Road, Chengdu 610065, China

[2] School of Chemistry and Chemical Engineering, South China University of Technology, Guangzhou 510640, China

[3] Institute for Superconducting and Electronic Materials, University of Wollongong, Wollongong, NSW 2522, Australia

Introduction

Renewable and sustainable energy resources, such as solar, wind, and tide, attract more and more attention because of the quick decrease of fossil fuels and the urgent need to address the environmental problems associated with their use [1–4]. However, these renewable energy resources are only intermittently available and require energy storage systems to improve the power reliability and quality [5, 6]. Lithium ion batteries (LIBs) with high energy density, superb rate capability, and satisfactory lifetime have recently shown potential applications in the areas of electric vehicles and stationary energy storage for smart grids [7–9]. To extend the operation hours of mobile IT devices and the driving mileages of all-electric vehicles, the energy densities of LIBs still require further extensive improvement [2, 6]. High-voltage LiNi$_{0.5}$Mn$_{1.5}$O$_4$ (LNMO), as a derivative of the spinel LiMn$_2$O$_4$, has been considered as one of the hottest cathode candidates, due to the theoretical capacity of 146.7 mA h g^{-1}, cubic spinel structure, good electrochemical performance, low cost of raw material, and environmentally friendly properties [10–14]. Furthermore, it shows 20 and 30 % higher energy density than conventional LiCoO$_2$ and LiFePO$_4$, respectively [15, 16].

Apart from the inherent properties of the material, other attributes, including the crystallinity, particle morphology, phase purity, and cation disordering are also important and should be optimized [17–19]. The synthetic route is one of the main reasons to greatly affect them in the structure of the cathodes. Therefore, different synthesis methods have been devoted to addressing these obstacles, such as the solid-state, liquid co-precipitation, sol-gel, and template methods [18–23]. LNMO products with various morphologies and particle sizes ranging from nanometers to microns have been synthesized by these techniques. In particular, carbonate co-

precipitation is regarded as one of the most effective ways to prepare various morphologies and excellent electrochemical performance of materials [12]. Among the various structured electrode materials, hollow structures with well-defined morphology, composition, and interior have attracted intense attention in recent years [20–23]. Generally, hollowing the electrode materials with well-defined nano-architectures may contribute to the improved electrochemical performance. The cavity in each hollow sphere can provide many extra active sites for the storage of Li^+, which is beneficial for enhancing the specific capacity. In addition, the hollow structure made of nanoparticles often has a larger surface area and a reduced effective diffusion distance for Li^+, leading to improved rate capability. Most importantly, the void space in the hollow sphere may buffer against the local volume change during the lithium insertion/extraction cycling, thus facilitating the structural stability of the electrode material and improving the cyclability [21–25]. Considering the particular advantages of hollow structures, LNMO hollow structures would be a very attractive cathode material for LIBs. Up to now, the common approaches for the synthesis of LNMO hollow structures are mostly template-directed methods [26]. However, template routes exhibit complicated procedures and high cost. Also, they are not practical for LIBs with mass production. Hence, a simple and low-cost method for synthesis of LNMO hollow structures is needed.

Herein, the study presents a facile co-precipitation strategy to fabricate hollow LNMO microspheres for LIB applications. The preparation processes start from the nickel manganese carbonate microspheres, which are prepared through a co-precipitated reaction. Then, the $(Ni_{0.25}Mn_{0.75})CO_3$ precursors directly blend with a stoichiometric amount of Li_2CO_3, and calcine in air to obtain the final products, which show good electrochemical performances such as specific capacity, rate capability, and cycling stability.

Experimental

Sample preparation

All the chemical reagents were analytical grade without further purification. Spherical $(Ni_{0.25}Mn_{0.75})CO_3$ precursors were prepared by a simple carbonate co-precipitation method. In specific, an aqueous solution of $NiSO_4$ and $MnSO_4$ (cationic ratio of Ni/Mn = 1:3) with a concentration of 2.0 mol L^{-1} was added dropwise to a tank reactor under vigorous stirring. At the same time, Na_2CO_3 solution (aq.) of 2.0 mol L^{-1} and desired amount of NH_4OH solution were also separately fed into the reactor. The reaction temperature was controlled at 52 °C. The pH value of the mixed solution was controlled between 7 and 8 during the precipitation process. The precursor was collected, washed with water several times to remove residual sodium and sulfuric species, and dried inside a vacuum oven set at 80 °C for 12 h.

Synthesis of hollow LNMO (marked as NM-H) microspheres contains multi-step process and rather complicated reactions in the high-temperature range. To give a clear and simple instruction, we roughly designed several steps which were carried out to get the final product in Fig. 1. In step I, the obtained $(Ni_{0.25}Mn_{0.75})CO_3$ precursor was mixed with a stoichiometric amount of Li_2CO_3 (5 % excess lithium source was added in order to make up for the volatilization of lithium during calcination). In step II, the mixture calcined in air at 500 °C for 5 h. It could involve the following processes: (1) $6(Ni_{0.25}Mn_{0.75})CO_3 + O_2 \rightarrow 2(Ni_{0.25}Mn_{0.75})_3O_4 + 6CO_2$ and (2) $(Li_2CO_3 \rightarrow Li_2O + CO_2)$. Then, the intermediate product was calcined at 900 °C for 12 h. The final lithiation procedure of the fabrication for hollow NM-H microspheres can be illustrated briefly as follows: $(8(Ni_{0.25}Mn_{0.75})_3O_4 + 6Li_2O + 5O_2 \rightarrow 12LiNi_{0.5}Mn_{1.5}O_4)$.

Material characterization

Thermogravimetric analysis was operated on a thermogravimetric analyzer (NETZSCH, TGA 209F1) with a heating rate of 10 °C min^{-1} to determine the mass loss and thermal behaviors. Crystalline phases of the synthesized materials were identified by x-ray diffraction (XRD, D/max-rB, Rigaku, Japan) measurements using Cu-Kα radiation in the 2θ range of 10°–80° at a continuous scan mode with a step size of 0.02° for a counting time of 10 s. Particle morphologies were observed by scanning electron microscope (SEM, JSM-5900LV), field-emission transmission electron microscopy (TEM), and high-resolution transmission electron microscopy (HRTEM) on a JEM-2100 instrument.

Electrochemical tests

The electrochemical characterizations of the LNMO powders were carried out under ambient temperature using CR2025 coin-type half cells. The cell contains a cathode, a lithium metal anode, and a porous polypropylene film Celgard 2400, which was used to separate the cathode and anode. Then, 1 mol L^{-1} $LiPF_6$ dissolved in a mixture of ethylene carbonate and dimethyl carbonate (1:1 by volume) was used as the electrolyte. The prepared LNMO powders, acetylene black, and polyvinylidene fluoride (PVDF, binder) were mixed at a mass ratio of 80:13:7 in 1-methyl-2-pyrrolidinone (NMP). The mixed slurry was spread on an aluminum foil and dried in a vacuum oven at 120 °C for 10 h. The loading of the active material in the electrode was 3–4 mg cm^{-2}. The cell was charged with a constant current to the 5.0 V and then charged with constant voltage for an hour. After that, cells were discharged with constant current densities (1 C = 147 mA g^{-1}) to the 3.6 V on a battery test device

Fig. 1 Schematic illustration of the synthesis route for the NM-H sample via co-precipitation method combined with a calcination process
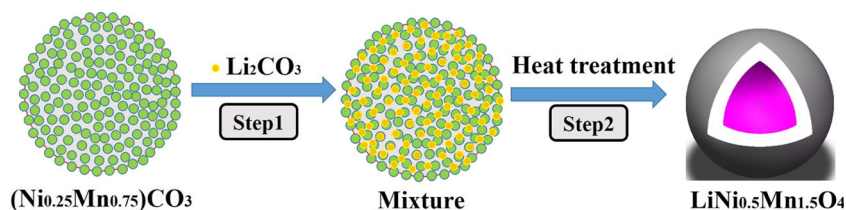
(Neware BTS-610). The cyclic voltammetry was taken at a scan rate of 0.1 mV s^{-1} between 3.6 and 5.0 V (vs. Li/Li$^+$). Electrochemical impendence spectroscopy (EIS) measurements were taken with an electrochemical workstation of type CHI660C over the frequency range of 100 kHz-10 mHz with the amplitude of 5 mV at room temperature.

Results and discussion

Figure 2 shows the XRD patterns of the spherical $(Ni_{0.25}Mn_{0.75})CO_3$ precursor and hollow NM-H microspheres. From Fig. 2a, we can see that the diffraction peaks of precursor can be readily indexed to a typical hexagonal carbonate structure with a space group of R-3c, which are almost consistent with that of iso-structural $MnCO_3$ (JCPDS#44-1472). Obviously, there also exist the diffraction peaks of $NiCO_3$ (JCPDS card no. 12-0771, marked with an asterisk). In addition, the diffraction peaks are broadened due to the spherical secondary particles composed of a lot of nanosized primary particles [18, 20]. We can also see that all the strong diffraction peaks of the NM-H are well indexed to the structure of spinel phase (JCPDS card No. 80-2162) with a space group of Fd-3m (Fig. 2b). Besides, weak diffraction peak at $2\theta = 43.6°$, as marked with asterisks, can be ascribed to the rock salt phase $Li_xNi_{1-x}O$, due to the lithium loss during high-temperature calcination [23, 24]. According to previous reports [27], the content of impurity phase is estimated by calculating the ratio of peak intensity at $2\theta = 43.6°$ of impurity phase to that at $2\theta = 44.3°$ of spinel phase. The intensity ratio in the NM-H is 6.5:100, which can be negligible. It indicates that the NM-H sample has a low impurity, which is believed to be beneficial to the electrochemical properties. Because the existence of impurity phase will accelerate the formation of

defects in the crystal, the mobility of Li$^+$ in the high impurity sample would be hindered. What's more, a high Mn^{3+} content induced by a high impurity could generate Jahn-Teller distortion and Mn^{2+} dissolution into the electrolyte, leading to poor performances [24–26].

In order to confirm the accurate reaction temperature for the phase formation of the NM-H sample, thermogravimetric analysis of the precursor was conducted in air. The obtained TG and TGA curves are depicted in Fig. 3; we can see that three distinct regions of weight loss are exhibited in the regions of 30–185, 285–535, and 550–800 °C. The first weight loss region, i.e., before 185 °C is ascribed to the evaporation of adsorbed moisture (ca. 7.02 %). The second weight loss (around 31.01 %) between 285 and 535 °C is attributed to the decomposition of $(Ni_{0.25}Mn_{0.75})CO_3$ and Li_2CO_3. The final weight loss from 550 to 800 °C corresponds to the formation of NM-H with spinel structure. However, precursor with a small amount (~0.5 mg) was used to investigate reaction temperature for the phase formation. Considering the relatively large quantity of the sample and reaction kinetics during the real calcination process, a higher temperature of 900 °C was set to guarantee the complete decomposition of the precursor and the high crystallinity of the final product.

Generally, the spinel LNMO has two different space groups: $P4_332$ group with Mn and Ni ions ordering in the 12d and 4a sites and Fd-3m group with random occupation of Mn and Ni ions in the 16d octahedral sites. Raman spectroscopy can be employed to distinguish between the disordered Fd-3m and ordered $P4_332$ space groups [27, 28]. The Raman spectrum of the NM-H sample was measured and shown in Fig. 4. According to previous reports, the strongest peak in NM-H is at around 630 cm^{-1} and can be assigned to the symmetric Mn-O stretching mode of MnO_6 octahedra (A$_{1g}$), while the two bands at around 394 and 490 cm^{-1} are

Fig. 2 XRD patterns of $(Ni_{0.25}Mn_{0.75})CO_3$ (**a**) and the NM-H sample (**b**)
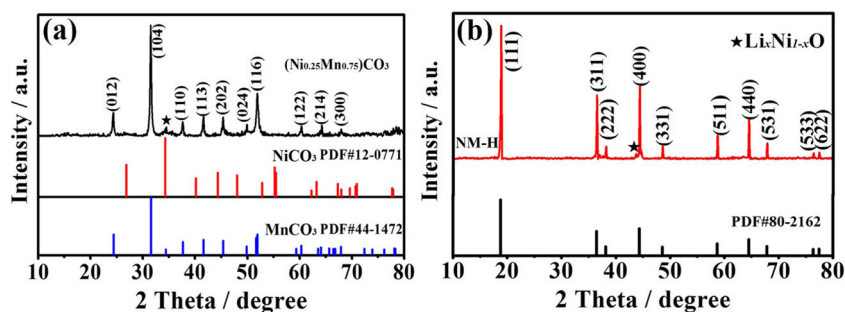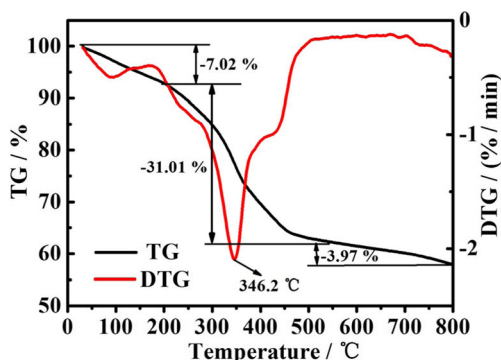
Fig. 3 Thermal gravimetric (TG) and differential thermal gravimetry (DTG) curves of the NM-H sample
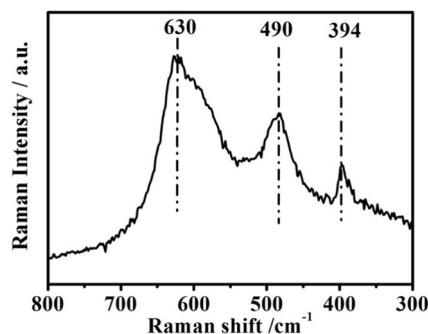

Fig. 4 Raman spectra of the NM-H sample

associated with the Ni-O stretching mode in the crystallite structure. The splitting of the T2g$^{(3)}$ band near 580–606 cm^{-1}, obvious evidence of the ordered structure of $P4_332$ for the spinel, is absent in the Raman spectrum of NM-H sample [24, 27]. Therefore, the peaks are the fingerprints of the Fd-$3m$ phase in NM-H rather than the $P4_332$ phase, which is consistent with the information obtained from the XRD pattern. It has been reported that LNMO with the Fd-$3m$ space group shows better electrochemical performance than the spinel with the $P4_332$ space group due to 2.5 orders

of magnitude faster electronic conductivity caused by the higher electron conduction between mixed Mn$^{3+/4+}$ cations [28, 29].

Particle morphologies under different magnifications of precursors and final products were investigated by scanning electron microscopy (SEM). Figure 5a, b illustrates typical SEM images of spherical (Ni$_{0.25}$Mn$_{0.75}$)CO$_3$ precursors with diameters of 2–3 μm. Moreover, the high magnification image focusing on the surface of a single microsphere reveals that the microsphere is closely constituted by a host of nanoparticles and nanosheets (Fig. 5c). From the image of the NM-H sample in Fig. 5d, e, we can see that the sample is hollow hierarchical structure with a size around 2 μm, similar to the (Ni$_{0.25}$Mn$_{0.75}$)CO$_3$ spheres. The magnified region of a single microsphere (Fig. 5f) reveals that the microsphere is composed of regular octahedral nanoparticles in the range of 100–350 nm. On the other hand, the dimension of the primary particle has somewhat grown compared to that in the precursor because lithiation reaction happens and crystal growth occurs at high temperature [11].

TEM and HRTEM images can provide more insight into the microstructure of the products and further confirm hollow structure. In Fig. 6a, b, a distinct light–dark contrast is observed in the spheres, suggesting their hollow nature. The formation of the hollow structure is attributed to the decomposition of the carbonate precursors to release CO$_2$ and the Kirkendall effect, which refers to unequal directional matter flows in a diffusion couple [21, 24]. During lithiation, the fast outward diffusion of Ni and Mn atoms and the slow inward diffusion of O atoms form a hollow cavity [21]. Meanwhile the high-resolution TEM image for the NM-H sample shown in Fig. 6c displays the periodic lattice fringe spacing with approximate value of 0.47 nm, which matches the interspaces of (111) of the cubic spinel LNMO (JCPDS Card no. 80-2162), and reveals the high crystallinity of the NM-H sample. What's more, the ordered lattices in a long-range order result in the easy occurrence of Li$^+$ intercalation/deintercalation,
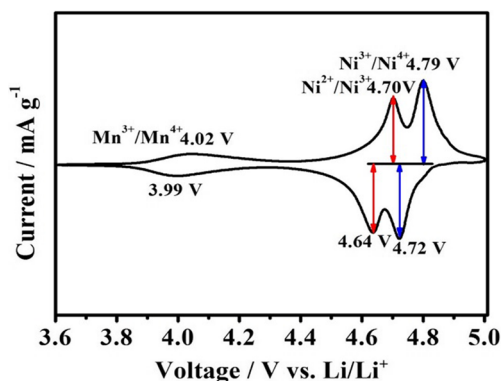
Fig. 5 SEM images under different magnifications of spherical (Ni$_{0.25}$Mn$_{0.75}$)CO$_3$ precursor (**a**–**c**) and the NM-H sample (**d**–**f**)
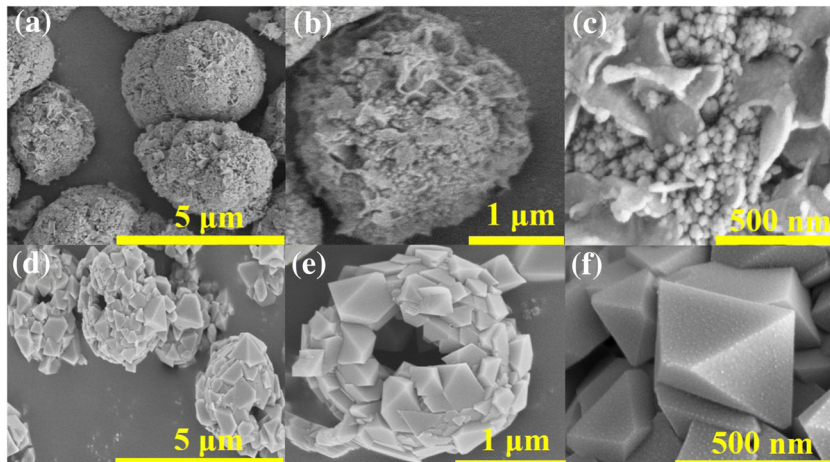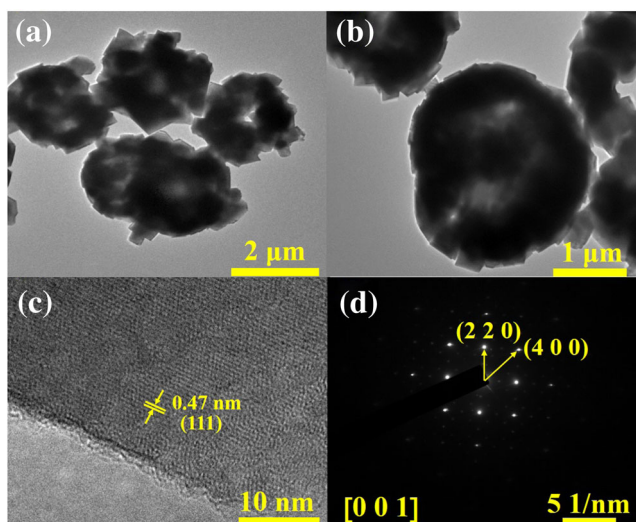
Fig. 6 The NM-H sample of TEM images (**a**, **b**), HRTEM image (**c**), and SAED pattern (**d**)

Fig. 7 Cyclic voltammetry curve of the NM-H sample

which is favorable for the rate capability. In addition, selected-area electron diffraction pattern (Fig. 6d) presents a well-organized array of diffraction spots that reveal the single-crystalline characteristic of the subunits and a cubic spinel structure [24].

The electrochemical performances of the as-prepared hollow NM-H microspheres were studied subsequently. Cyclic

voltammetry was applied to study the oxidation/reduction behavior of the NM-H sample. Generally, LNMO with the $P4_332$ space group shows only a strong oxidation peak at around 4.7 V corresponding to the Ni^{2+}/Ni^{4+} redox couple [26, 27]. However, from Fig. 7, we can see that a pair of minor oxidation/reduction peaks appears near 4.0 V, which can be attributed to the redox reaction of the Mn^{3+}/Mn^{4+} couple. And the oxidation peak splits into two separate peaks because of the voltage difference between Ni^{2+}/Ni^{3+} and Ni^{3+}/Ni^{4+} redox couples. This finding suggests that NM-H sample exhibits the Fd-3m space group, in accordance with the Raman result. It is generally accepted that the polarization degree can be measured by the potential difference between the anodic and cathodic peaks of LNMO. The potential difference between the anodic and cathodic peaks of Ni^{2+}/Ni^{3+} and Ni^{3+}/Ni^{4+} are 0.06 and 0.07 V, respectively, which are lower than the previous reports [26, 27]. This observation indicates that hollow structure is beneficial to the reversible intercalation/deintercalation of Li^+.

Figure 8a exhibits the charge-discharge curves of the initial 10 cycles at 0.5 C in the voltage window of 3.6–5.0 V. It can be seen that the NM-H exhibits a highly stable discharge specific capacity of ~138.2 mA h g^{-1} and the corresponding discharge specific energy is ~628 Wh kg^{-1}. Also, charge-discharge curves with different charge-discharge times at 0.5 C are shown in Fig. 8b. They show a steady larger plateau in the 4.7 V region and a smaller plateau about at 4.0 V, which are attributed to Ni^{2+}/Ni^{4+} and Mn^{3+}/Mn^{4+} redox reactions, respectively [30–32].

Charge and discharge profiles and rate capability of the NM-H sample at different rates are shown in Fig. 9. The electrode was charged and discharged at the same rate from 0.5 to 1 C, and then charged at 1 C for each charging process and discharged at various rates from 3 to 20 C. It delivers good rate capability with discharge capacities of 138.2 (0.5 C), 129.8 (1 C), 122.3 (3 C), 117.8 (5 C), 108.5 (10 C), and 92.6 mAh g^{-1} (20 C), especially 138.2 mAh g^{-1} at 0.5 C, which is close to the theoretical capacity of LNMO (147 mAh g^{-1}). However, it can be noticed that the capacity of NM-H decays at high discharge rate and discharge plateau

Fig. 8 Charge-discharge profiles of the initial 10 cycles (**a**) and charge-discharge curves with different charge-discharge times (**b**) of the NM-H sample at 0.5 C
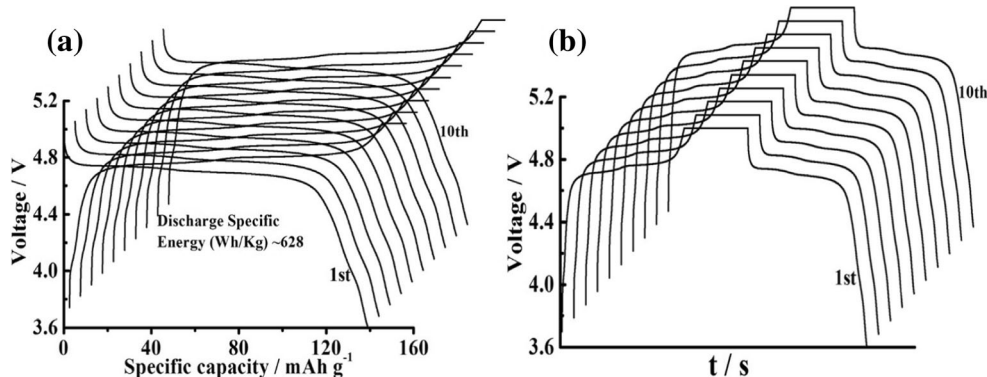
Fig. 9 Charge and discharge profiles (**a**) and rate capability (**b**) of the NM-H sample at different rates in voltage of 3.6–5.0 V
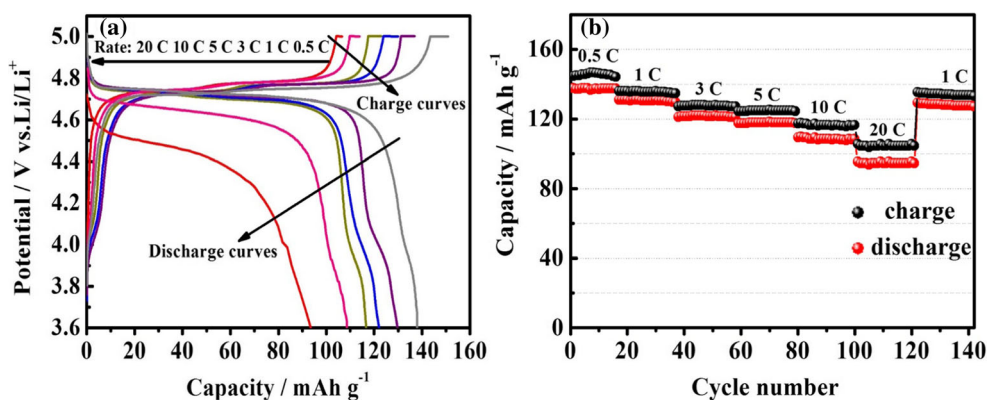

Fig. 10 Cycling performance (**a**) and capacity retention at selected cycles (**b**) of the NM-H sample with charge rate at 1 C and discharge rate at 1, 5, and 10 C
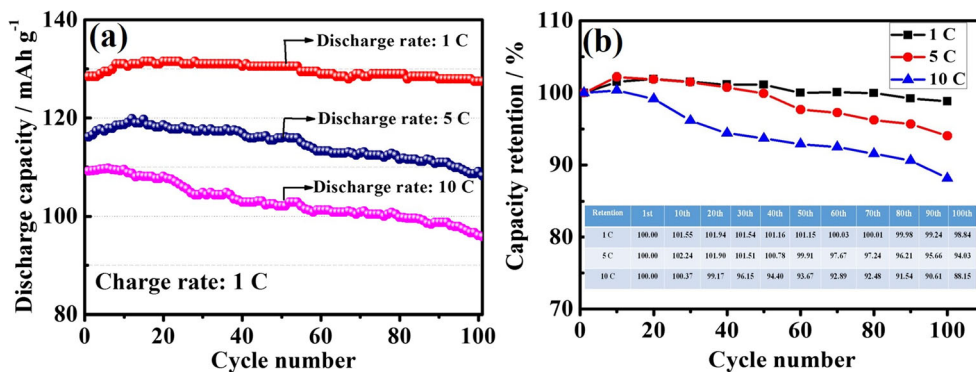

becomes shorter and almost disappears at 20 C, which mainly attribute to the surface polarization caused by the side-reactions between electrode and electrolyte [33–35]. Figure 9b shows that the storage capacity is stable at each current rate. It is worthy to note that the specific capacity almost returns to its original value soon after the rate reverses back to 1 C, revealing the superior reversibility of the NM-H sample.

Figure 10 illustrates the cycling performance and capacity retention at selected cycles of the NM-H sample with charge rate at 1 C and discharge rate at 1, 5, and 10 C. The initial discharge capacities of 128.5, 116.7, and 109.2 mAh g^{-1} can be obtained at 1, 5, and 10 C, respectively. After 100 cycles, the corresponding capacity retention rates are 98.8, 94.0, and 88.2 %, showing the potential in the application of high rate discharge. Also, the specific capacity retentions at selected cycles of the sample are summarized in the table of Fig. 10b. Compared with the previous studies [18, 28], NM-H exhibits both higher capacity and better cyclic stability. On the other hand, it is well known that one of the main drawbacks of LNMO materials is the inferior cycling stability at elevated temperature. In this work, we also investigated the cycling performance of the NM-H sample at 55 °C, as shown in Fig. 11. It displays good

cycling stability at elevated temperature. The discharge capacity reaches its maximum value of 122.1 mAh g^{-1} at the eighth cycle under 5-C discharge rate. The NM-H sample delivers an initial discharge capacity of 118.8 mAh g^{-1}, and still retains 85.7 % of the initial capacity after 100 cycles. The remarkable electrochemical performances might be related to the peculiar structures. The hollow structure in the interior could provide many extra active sites for the storage of Li$^+$ and allow for the full contact of the particles with the electrolyte. In addition, the special structures could significantly
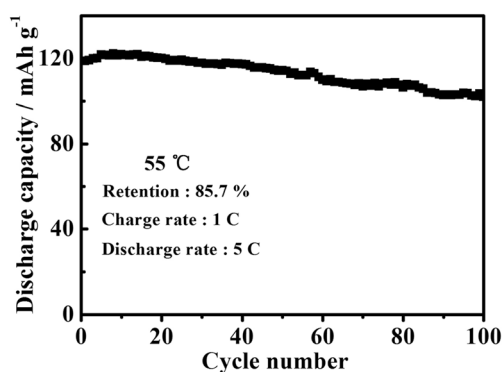
Fig. 11 Cycling performance of the NM-H sample with charge rate at 1 C and discharge rate at 5 C at 55 °C
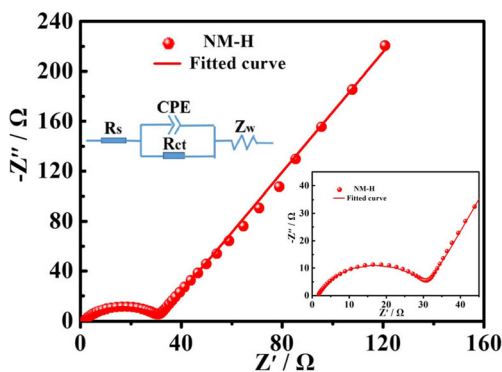
Fig. 12 Nyquist impedance spectra and equivalent circuit of the NM-H sample at room temperature

improve the structural integrity by partly mitigating the mechanical strain induced by volume change associated with the repeated lithium ion intercalation/deintercalation processes during cycling [20–23].

To understand the kinetic behaviors of lithium ion in the material, hollow NM-H sample was further investigated by electrochemical impedance spectrum (EIS) measurements. Figure 12 shows the Nyquist plot of the electrode measured after 30 charge-discharge cycles at 1 C and fitted curve using Zview software. The plot consists of a depressed semicircle at high frequency relating to the charge transfer resistance (R_{ct}) and a sloping line in the low frequency region ascribing to the diffusion of lithium ion in the sample, which is highly consistent with the previous studies [36–38]. The value of R_{ct} fitted by the equivalent circuit inserted in Fig. 11 is 28.65 Ω, which is lower than the previous report [11]. It indicates the fast transport of charged species between the electrode and electrolyte.

Conclusion

In summary, hierarchical hollow $LiNi_{0.5}Mn_{1.5}O_4$ microspheres as a 5-V cathode material for lithium ion batteries has been synthesized by a co-precipitation approach accompanied with high-temperature calcinations. Such peculiar structure could provide many extra active sites for the storage of Li$^+$, allowing for the full contact with the electrolyte and release the stress resulting from the volume change during the charge-discharge processes. The obtained products deliver enhanced electrochemical performances with good rate capability and cycle stability, which makes it a promising cathode candidate for high-energy density lithium ion batteries. Furthermore, we believe that this process can be applied for preparation of other hierarchical hollow electrode materials with improved electrochemical performances.

References

1. Zhang J, Wu Z, Hua W, Liu H, Zhong B (2015) High-performance porous spherical cathode materials based on CaCO$_3$-template synthesis of $LiNi_{1/3}Co_{1/3}Mn_{1/3}O_2$ for lithium-ion batteries. Ionics 21: 3151–3158
2. Xu R, Zhang X, Chamoun R, Shui J, Li JCM, Lu J, Amine K, Belharouak I (2015) Enhanced rate performance of $LiNi_{0.5}Mn_{1.5}O_4$ fibers synthesized by electrospinning. Nano Energy 15:616–624
3. Zhang L, Wu B, Li N, Mu D, Zhang C, Wu F (2013) Rod-like hierarchical nano/micro $Li_{1.2}Ni_{0.2}Mn_{0.6}O_2$ as high performance cathode materials for lithium-ion batteries. J Power Sources 240: 644–652
4. Zhang L, Borong W, Ning L, Feng W (2014) Hierarchically porous micro-rod lithium-rich cathode material $Li_{1.2}Ni_{0.13}Mn_{0.54}Co_{0.13}O_2$ for high performance lithium-ion batteries. Electrochim Acta 118: 67–74
5. Sun S, Du C, Qu D, Zhang X, Tang Z (2015) Li_2ZrO_3-coated $LiNi_{0.6}Co_{0.2}Mn_{0.2}O_2$ for high-performance cathode material in lithium-ion battery. Ionics 21:2091–2100
6. Feng J, Huang Z, Guo C, Chernova NA, Upreti S, Whittingham MS (2013) An organic co-precipitation route to synthesize high voltage $LiNi_{0.5}Mn_{1.5}O_4$. ACS Appl Mater Interfaces 5:10227–10232
7. Li L, Wang L, Zhang X, Xie M, Wu F, Chen R (2015) Structural and electrochemical study of hierarchical $LiNi_{1/3}Co_{1/3}Mn_{1/3}O_2$ cathode material for lithium-ion batteries. ACS Appl Mater Interfaces 7:21939–21947
8. Yan J, Liu H, Wang Y, Zhao X, Mi Y, Xia B (2015) Enhanced high-temperature cycling stability of $LiNi_{1/3}Co_{1/3}Mn_{1/3}O_2$-coated $LiMn_2O_4$ as cathode material for lithium ion batteries. Ionics 21: 1835–1842
9. Shi H, Wang X, Hou P, Zhou E, Guo J, Zhang J, Wang D, Guo F, Song D, Shi X, Zhang L (2014) Core–shell structured $Li[(Ni_{0.8}Co_{0.1}Mn_{0.1})_{0.7}(Ni_{0.45}Co_{0.1}Mn_{0.45})_{0.3}]O_2$ cathode material for high-energy lithium ion batteries. J Alloy Compd 587:710–716
10. Wen W, Chen S, Fu Y, Wang X, Shu H (2015) A core–shell structure spinel cathode material with a concentration-gradient shell for high performance lithium-ion batteries. J Power Sources 274:219–228
11. Pan J, Deng J, Yao Q, Zou Y, Wang Z, Zhou H, Sun L, Rao G (2015) Novel $LiNi_{0.5}Mn_{1.5}O_4$ porous microellipsoids as high-performance cathode materials for lithium ion batteries. J Power Sources 288:353–358
12. Wen W, Wang X, Chen S, Shu H, Yang X (2015) Design and preparation of spherical high voltage $LiNi_{0.5}Mn_{1.5}O_4$ with a novel concentration-gradient shell for lithium ion batteries. J Power Sources 281:85–93
13. Xue L, Liao Y, Yang L, Li X, Li W (2014) Improved rate performance of $LiNi_{0.5}Mn_{1.5}O_4$ cathode for lithium ion battery by carbon coating. Ionics 21:1269–1275
14. Boesenberg U, Falk M, Ryan CG, Kirkham R, Menzel M, Janek J, Fröba M, Falkenberg G, Fittschen UEA (2015) Correlation between chemical and morphological heterogeneities in $LiNi_{0.5}Mn_{1.5}O_4$ spinel composite electrodes for lithium-ion batteries determined by micro-X-ray fluorescence analysis. Chem Mater 27:2525–2531

15. Shu H, Wang X, Wu Q, Hu B, Yang X, Wei Q, Liang Q, Bai Y, Zhou M, Wu C, Chen M, Wang A, Jiang L (2013) Improved electrochemical performance of LiFePO$_4$/C cathode via Ni and Mn co-doping for lithium-ion batteries. J Power Sources 237:149–155

16. Wan L, Deng Y, Yang C, Xu H, Qin X, Chen G (2015) Ni/Mn ratio and morphology-dependent crystallographic facet structure and electrochemical properties of the high-voltage spinel LiNi$_{0.5}$Mn$_{1.5}$O$_4$ cathode material. RSC Adv 5:25988–25997

17. Zhao H, Li F, Liu X, Xiong W, Chen B, Shao H, Que D, Zhang Z, Wu Y (2015) A simple, low-cost and eco-friendly approach to synthesize single-crystalline LiMn$_2$O$_4$ nanorods with high electrochemical performance for lithium-ion batteries. Electrochim Acta 166:124–133

18. Liu X, Li D, Mo Q, Guo X, Yang X, Chen G, Zhong S (2014) Facile synthesis of aluminum-doped LiNi$_{0.5}$Mn$_{1.5}$O$_4$ hollow microspheres and their electrochemical performance for high-voltage Li-ion batteries. J Alloy Compd 609:54–59

19. Li J, Xiong S, Liu Y, Ju Z, Qian Y (2013) Uniform LiNi$_{1/3}$Co$_{1/3}$Mn$_{1/3}$O$_2$ hollow microspheres: designed synthesis, topotactical structural transformation and their enhanced electrochemical performance. Nano Energy 2:1249–1260

20. Deng S, Mao D, Wang H, Wang B, Liu J, Ma Y, Yan H (2016) Preparation and electrochemical properties of double-shell LiNi$_{0.5}$Mn$_{1.5}$O$_4$ hollow microspheres as cathode materials for Li-ion batteries. RSC Adv 6:45369–45375

21. Zhou L, Zhao D, Lou X (2012) LiNi$_{0.5}$Mn$_{1.5}$O$_4$ hollow structures as high-performance cathodes for lithium-ion batteries. Angew Chem Int Ed 124:243–245

22. Zhou L, Zhao D, Lou X (2012) Double-shelled CoMn$_2$O$_4$ hollow Microcubes as high-capacity anodes for lithium-ion batteries. Adv Mater 24:745–748

23. Wu W, Xiang H, Zhong G, Su W, Tang W, Zhang Y, Yu Y, Chen C (2014) Ordered LiNi$_{0.5}$Mn$_{1.5}$O$_4$ hollow microspheres as high-rate 5 V cathode materials for lithium ion batteries. Electrochim Acta 119:206–213

24. Luo H, Nie P, Shen L, Li H, Deng H, Zhu Y, Zhang X (2015) Synthesis of LiNi$_{0.5}$Mn$_{1.5}$O$_4$ hollow microspheres and their lithium-storage properties. ChemElectroChem 2:127–133

25. Wang Z, Zhou L, Lou X (2012) Metal oxide hollow nanostructures for lithium-ion batteries. Adv Mater 24:1903–1911

26. Zhu C, Akiyama T (2016) Designed synthesis of LiNi$_{0.5}$Mn$_{1.5}$O$_4$ hollow microspheres with superior electrochemical properties as high-voltage cathode materials for lithium-ion batteries. RSC Adv 4:10151–10156

27. Xue Y, Wang Z, Zheng L, Yu F, Liu B, Zhang Y, Ke K (2015) Investigation on preparation and performance of spinel LiNi$_{0.5}$Mn$_{1.5}$O$_4$ with different microstructures for lithium-ion batteries. Sci Rep 5:13299

28. Wu W, Chen J, Cheng S, Xiang H (2015) Preparation and electrochemical performance of spinel LiNi$_{0.5-x}$ Mn$_{1.5+x}$ O$_4$ (x = 0, 0.05, 0.1) hollow microspheres as cathode materials for lithium-ion batteries. Ionics 21:1843–1849

29. Zhang X, Cheng F, Zhang K, Liang Y, Yang S, Liang J, Chen J (2012) Facile polymer-assisted synthesis of LiNi$_{0.5}$Mn$_{1.5}$O$_4$ with a hierarchical micro-nano structure and high rate capability. RSC Adv 2:5669–5675

30. Cabana J, Casas-Cabanas M, Omenya FO, Chernova NA, Zeng D, Whittingham MS, Grey CP (2012) Composition-structure relationships in the Li-ion battery electrode material LiNi$_{0.5}$Mn$_{1.5}$O$_4$. Chem Mater 24:2952–2964

31. Zhang X, Cheng F, Yang J, Chen J (2013) LiNi$_{0.5}$Mn$_{1.5}$O$_4$ porous nanorods as high-rate and long-life cathodes for Li-ion batteries. Nano Lett 13:2822–2825

32. Gao J, Li J, Song F, Lin J, He X, Jiang C (2015) Strategy for synthesizing spherical LiNi$_{0.5}$Mn$_{1.5}$O$_4$ cathode material for lithium ion batteries. Mater Chem Phys 152:177–182

33. Chen Z, Zhao R, Li A, Hu H, Liang G, Lan W, Cao Z, Chen H (2015) Polyhedral ordered LiNi$_{0.5}$Mn$_{1.5}$O$_4$ spinel with excellent electrochemical properties in extreme conditions. J Power Sources 274:265–273

34. Kim JW, Kim DH, Oh DY, Lee H, Kim JH, Lee JH, Jung YS (2015) Surface chemistry of LiNi$_{0.5}$Mn$_{1.5}$O$_4$ particles coated by Al$_2$O$_3$ using atomic layer deposition for lithium-ion batteries. J Power Sources 274:1254–1126

35. Sun Y, Yang Y, Zhao X, Shao H (2011) Synthesis and electrochemical characterization of LiNi$_{0.5}$Mn$_{1.5}$O$_4$ by one-step precipitation method with ammonium carbonate as precipitating agent. Electrochim Acta 56:5934–5939

36. Luo D, Li G, Guan X, Yu C, Zheng J, Zhang X, Li L (2013) Novel synthesis of Li$_{1.2}$Mn$_{0.4}$Co$_{0.4}$O$_2$ with an excellent electrochemical performance from −10.4 to 45.4 °C. J Mater Chem A 1:1220–1227

37. Liu H, Zhu G, Zhang L, Qu Q, Shen M, Zheng H (2015) Controllable synthesis of spinel lithium nickel manganese oxide cathode material with enhanced electrochemical performances through a modified oxalate co-precipitation method. J Power Sources 274:1180–1187

38. Chemelewski KR, Lee E-S, Li W, Manthiram A (2013) Factors influencing the electrochemical properties of high-voltage spinel cathodes: relative impact of morphology and cation ordering. Chem Mater 25:2890–2897